Journal of Alloys and Compounds 509 (2011) 4367–4371

Contents lists available at ScienceDirect

Journal of Alloys and Compounds

journal homepage: www.elsevier.com/locate/jallcom

Electrochemical behaviors of SnO and Sn anodes for lithium rechargeable batteries

Young-Jun Kim [a], Min-Sik Park [a,*], Hun-Joon Sohn [b,*], Hyukjae Lee [c]

[a] Advanced Batteries Research Center, Korea Electronics Technology Institute, Seongnam, Gyeonggi 463-816, South Korea
[b] School of Materials Science and Engineering, Seoul National University, Seoul 151-744, South Korea
[c] Center for Green Materials Technology, School of Advanced Materials Engineering, Andong National University, Andong, Kyungbuk 760-745, South Korea

ARTICLE INFO

Article history:
Received 28 September 2010
Received in revised form
31 December 2010
Accepted 9 January 2011
Available online 15 January 2011

Keywords:
Tin oxides
Li rechargeable batteries
X-ray diffraction

ABSTRACT

Electrochemical behaviors of Sn and SnO anodes are studied. Charging/discharging curves show irreversible capacities at the first cycle in both Sn and SnO electrodes. The irreversible capacity loss in Sn electrode is due to the incomplete Li removal from Sn after the first cycle. Although the largest capacity loss in SnO electrode is a result from the lithia formation during the first discharge, additional capacity loss arises from the residual Li in metallic Sn owing to the aggregation of Sn upon repeated cycling. Contrary to the previous studies, $Li_{22}Sn_5$ phase is not observed in the discharge product in Sn and SnO electrodes. The LiSn alloy electrode shows almost 100% cycling efficiency at the first cycle due to the pre-existing Li.

1. Introduction

Tin based materials have been extensively exploited as substitutes for graphite which is widely used for anode in commercial lithium ion batteries. Metallic tin has a large theoretical capacity (992 mAh g^{-1}), that is much higher than graphite (372 mAh g^{-1}), via Li_xSn alloying and de-alloying reactions [1]. During charging, Li ions intercalate into the tin electrode forming various Li–Sn alloys from Sn-rich phase to Li-rich phase sequentially, and the reverse de-alloying reactions occur during discharging. These phase transitions during charging/discharging however result in enormous volume change (>300%) accompanying large mechanical strain which leads to pulverization of electrode and dramatic capacity fade upon cycling [2]. Tin oxide electrodes also have large theoretical capacities as compared to the graphite (SnO: 875 mAh g^{-1}, SnO_2: 783 mAh g^{-1}). During the first discharging, tin oxide is reduced to metallic tin while lithia forms from the reaction of Li with oxygen [3]. The metallic tin is dispersed in the lithia matrix and then reversibly reacts with Li to form a variety of Li_xSn alloys like tin electrode does. The lithia matrix can offer a facile environment for alloying/de-alloying reactions resulting in better cyclic performance of tin oxide electrode [4]. However, the irreversible capacity due to the lithia formation and quick capacity fade upon cycling, though better than pure metallic tin, hinder the practical use of tin oxide electrode [5].

There have been numerous studies about tin and tin oxide electrodes for lithium rechargeable batteries. However, most studies have focused on either the Li–Sn alloying/de-alloying processes or improvement of cycling performance via modification of electrode materials [6–11], and therefore there is a lack of interest in dissecting/understanding basic electrochemical behaviors in tin based compounds. The present study is a part of the work which aims to establish a firm understanding of tin based materials for lithium rechargeable batteries. In the present study, electrochemical behaviors of metallic tin and tin oxide electrodes are studied and compared using electrochemical measurements and X-ray diffraction analysis.

2. Experimental

All starting powders were obtained from Aldrich and Junsei Chemicals. LiSn powders were synthesized by mechanical milling of Li and Sn powders with a molar ration of 1:1. Stoichiometric amounts of Li (2–3 mm granular, 99.9%) and Sn (~325 mesh, 99.8%) were carefully weighed and sealed in the Ar-filled glove box to avoid undesirable oxidation. The mechanical milling process has been conducted in dry room for 6 h. Working electrode was prepared by the mixing of active powder (85 wt.%) with 10 wt.% carbon black as conducting agent and 5 wt.% polyvinylidene fluoride (PVDF) as binder in n-methyl-2-pyrrolidinone (NMP) solvent. The slurry was coated on copper foil. After evaporation of NMP, it was pressed and dried in vacuum oven at 120 °C for 6 h. The electrode was then cut into 1 cm diameter disk and moved into a glove box filled with argon where test cell was constructed. Li metal and poly-ethylene were used as the counter electrode and separator, respectively. 1 M $LiPF_6$ in ethy-

* Corresponding authors.
E-mail addresses: parkms@keti.re.kr, parkms@gmail.com (M.-S. Park).

0925-8388/$ – see front matter © 2011 Elsevier B.V. All rights reserved.
doi:10.1016/j.jallcom.2011.01.061

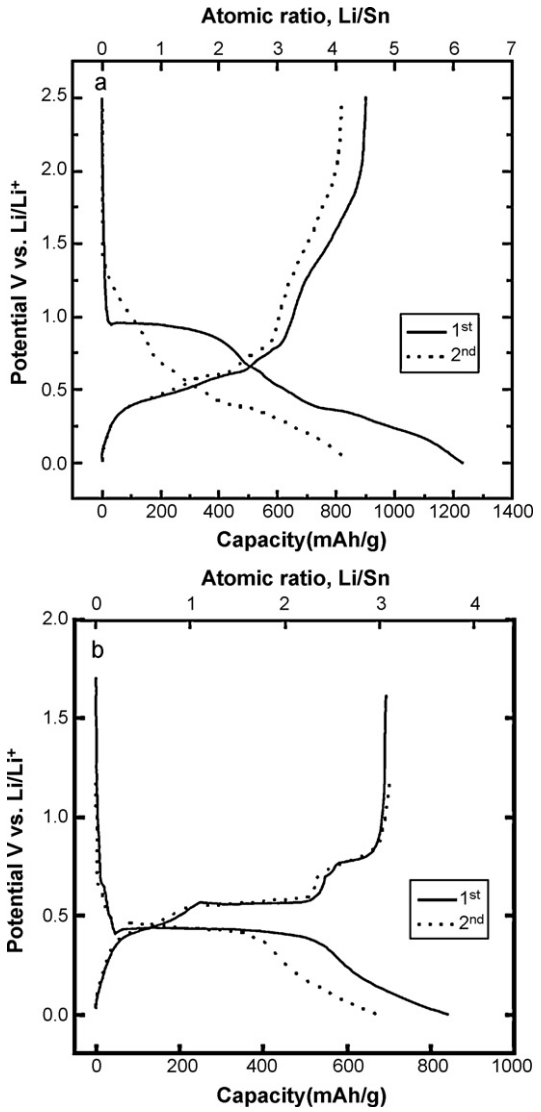

Fig. 1. Charge/discharge curves of SnO (a) and Sn (b) electrodes.

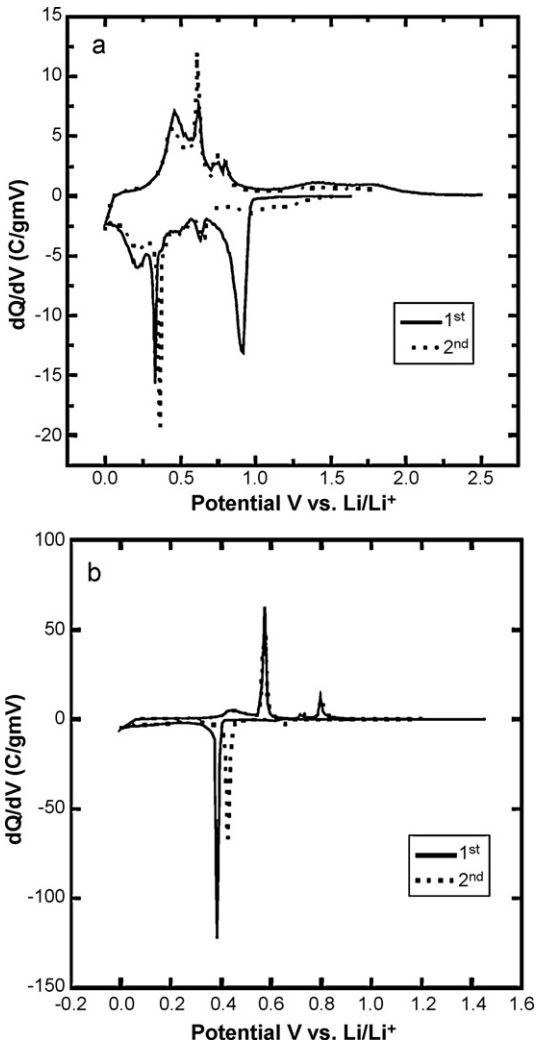

Fig. 2. Derivative capacity plots of SnO (a) and Sn (b) electrodes.

lene carbonate and diethylene carbonate (1:1 in volume) was also used for the electrolyte. Charge/discharge tests were conducted at a constant current in the range of 10 mA g^{-1} to 200 mA g^{-1} with various cut-off voltages. X-ray diffraction study was conducted using Cu K_α radiation with 60 kV acceleration voltage.

3. Results and discussion

The charge–discharge curves of SnO and Sn electrodes in the first two cycles are shown in Fig. 1. For SnO electrode, ~400 mAh g^{-1} irreversible capacity is observed in the first cycle. This irreversible capacity is caused by the bonding of two Li ions with oxygen from SnO to produce Li_2O and metallic Sn during the first discharge. Then, the metallic Sn reacts with Li ions reversibly to form various Li_xSn alloys by further discharge. The irreversible Li_2O formation is therefore the largest capacity loss for SnO electrode in the first cycle. Courtney and Dahn [3] reported that this reaction occurred at ~0.9 V. Similarly, about 400 mAh g^{-1} discharge capacity is observed between 1.0 and 0.8 V as shown in Fig. 1(a). Sn electrode also shows irreversible capacity in the first cycle, i.e., ~120 mAh g^{-1}. However, since there is no Li_2O formation in Sn electrode, the irreversible capacity in Sn electrode might be due to the incomplete removal of inserted Li in Sn during charging. The residual Li in Sn electrode would then be used for the formation of solid electrolyte interface (SEI) [12,13]. The amount of inserted Li into Sn during the first discharge is about 3.6–3.7 (Li/Sn atomic ratio) and the amount of Li released from Sn during the first charge is in a range of 3.0–3.1 (Li/Sn atomic ratio). After the first cycle, Sn electrode has almost 100% charge–discharge efficiency as shown in Fig. 1(b). It is to be noted here that the SnO electrode shows irreversible capacity in the second cycle either, although it is much smaller than that in the first cycle.

In the derivative capacity vs. potential plots (Fig. 2), a large peak for the SnO electrode at 0.9 V in discharge is ascribed to the formation of lithia which is irreversible reaction evidenced by the disappearance of the peak in the second cycle. This peak is not observed from Sn electrode as expected. Fig. 3 shows the XRD patterns for SnO electrode. Since the studies in Li–Sn alloying mechanism in tin based electrode have been reported extensively [3,6,14], only a few XRD patterns observed at important events are presented here for the sake of brevity. There are several distinct peaks in the derivative capacity plot in Fig. 2 and theses peaks are related to the phase transitions in SnO electrode. During discharging, metallic Sn emerges with the disappearance of SnO after the large peak at 0.9 V (B). Then Li–Sn alloy phases appear sequentially, starting from Sn-rich phase such as Li_2Sn_5 to Li-rich phases.

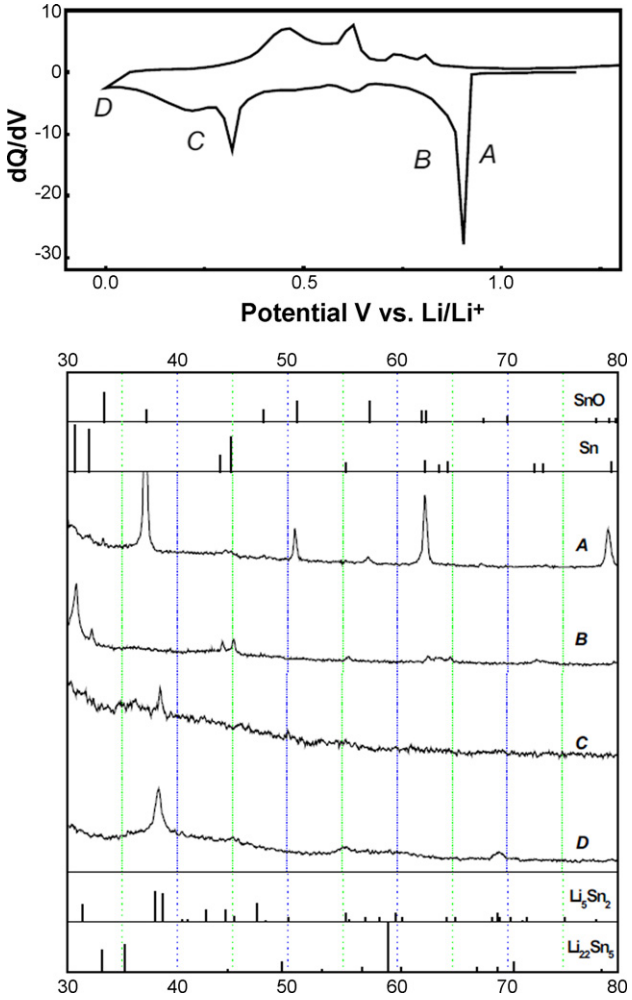

Fig. 3. XRD patterns of SnO electrode during the first discharge.

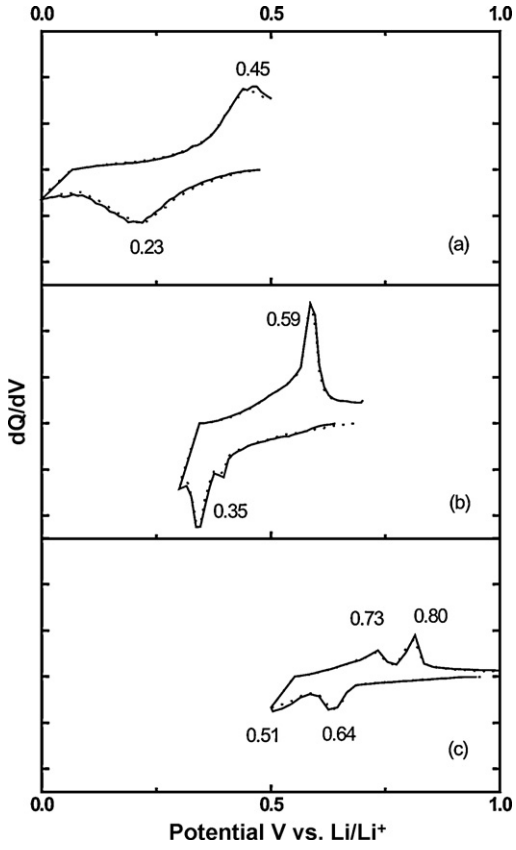

Fig. 4. Derivative capacity plots of SnO electrode over different voltage ranges: (a) 0.5–0.0 V, (b) 0.7–0.3 V, (c) 1.0–0.5 V (solid lines—2nd cycle and dotted lines—3rd cycle).

The final discharge product appears to be the mixture of Li_5Sn_2, $Li_{13}Sn_5$, and Li_7Sn_2 which are difficult to distinguish from each other due to the similarity of XRD patterns (D). Contrary to the previous report [3], which asserted that the final discharge product included $Li_{22}Sn_5$ phase, $Li_{22}Sn_5$ phase was not observed in the discharge product in the present study. In fact, the $Li_{22}Sn_5$ phase was not detected even after the discharged cell was intentionally short-circuited for 24 h. This implies that the theoretical capacity based on the formation of $Li_{4.4}Sn$ is impossible to reach for SnO electrode [3]. Since the reverse reactions occur during charging, the peaks in derivative capacity plot during charging are correlated to the peaks during discharging except the first peak in the first discharge which is for the irreversible lithia formation. Derivative capacity plots of SnO electrode over three different voltage ranges (Fig. 4) show that each peak in discharge has a corresponding peak in charge.

The alloy reactions in Sn and SnO electrodes can be compared using the derivative capacity plots in the first charge (Fig. 5). The number and position of peaks from two electrodes are almost identical even though intensity difference exists. Thus, it can be said that alloying and de-alloying mechanisms in the Sn electrode are similar to those in the SnO electrode, but poor crystallinity in SnO electrode causes the difference in intensity between them. In the XRD patterns from SnO electrode after the first and 10th cycles (Fig. 6), the metallic Sn peaks are more evident after 10 cycles. This indicates that Sn phase in SnO electrode has poor crystallinity

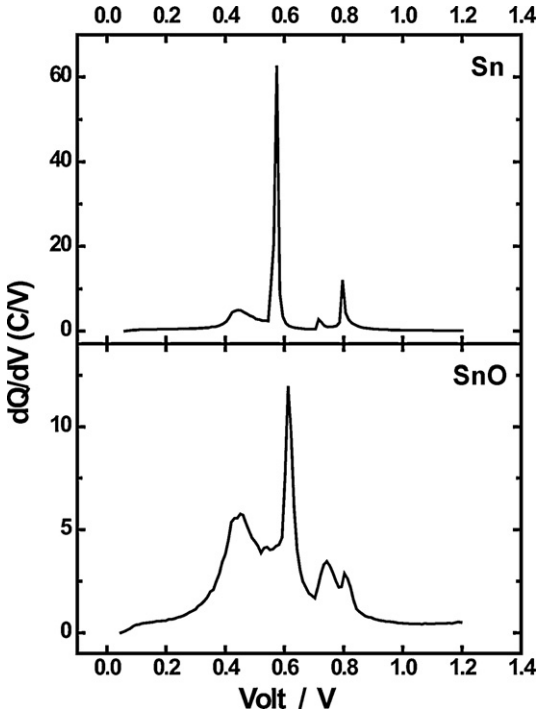

Fig. 5. Derivative capacity plots of Sn and SnO electrodes during the first charge.

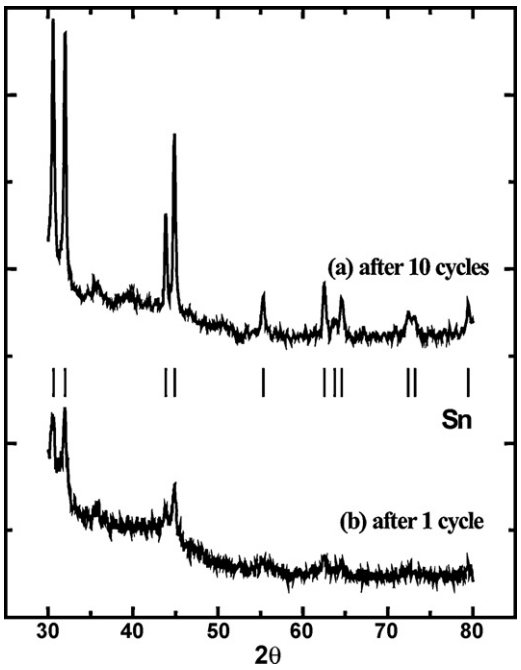

Fig. 6. XRD patterns of SnO electrode after 1 and 10 cycles.

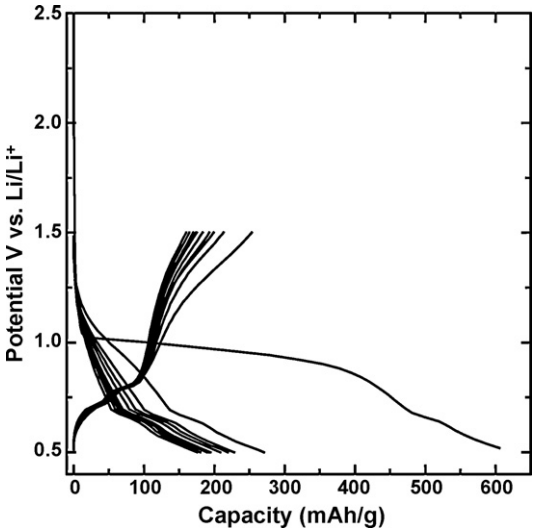

Fig. 8. Charge/discharge curves of SnO electrode cycled in the range of 0.5–1.5 V at the rate of 100 mA/g.

at the early cycles but the crystallinity develops with repeated cycling.

In Fig. 7, the cycling capacity of SnO electrode decreases dramatically with cycling. It is known that the main cause of the poor cyclability is a severe volume change during alloying/de-alloying processes in Li_xSn [5]. Therefore, a lift of the lower cutoff voltage should reduce the effect of volume change by preventing alloying/de-alloying processes. Figs. 8 and 9 show the charge–discharge curves and capacity vs. cycle number plot of SnO electrode when cycled in the range from 0.5 to 1.5 V at the rate of 100 mA/g, respectively. There are considerable capacity fade above 1.0 V. Further, the cycling capacity converges to a constant value after ~15–20 cycles. The difference in charge capacity between the first and 15th cycles is ~110 mAh g^{-1} which is comparable to the irreversible capacity due to the residual Li in Sn electrode after charge, i.e., ~120 mAh g^{-1} in Fig. 1(b). Fig. 10 shows the derivative capacity plot of SnO electrode which was cycled 30 times between 0.5 V and 1.5 V and then charged from 0 to 1 V. The peak intensities are significantly higher than those from virgin SnO electrode as shown in Fig. 2(a) such that overall shape looks more like Sn electrode, i.e., Fig. 5(b). Based on these results, it can be postulated that SnO electrode has similar properties to the metallic Sn via repeated cycling and it causes the capacity loss in SnO electrode above 1.0 V during the early cycling due to the residual Li in metallic Sn. Further, the amount of residual Li in SnO electrode reaches to that in Sn electrode after ~15–20 cycles where the plateau starts in Fig. 9. The reason for that SnO electrode behaves like Sn electrode with repeated cycling might be the aggregation of Sn in SnO electrode [3]. However, further study is necessary to fully clarify the Sn aggregation mechanism and the role of Sn aggregates in SnO electrode.

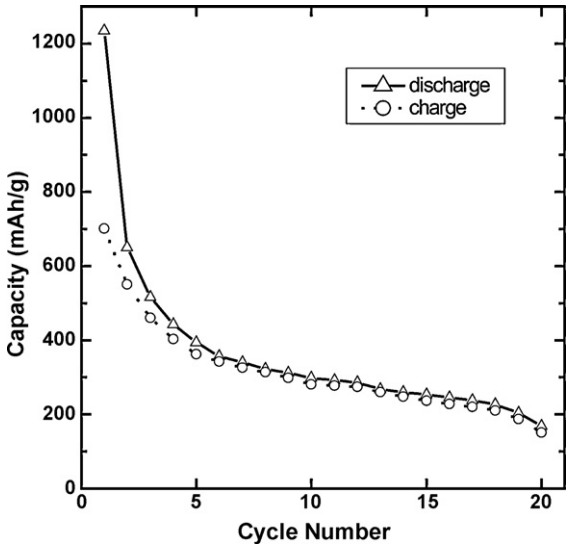

Fig. 7. The capacity vs. cycle number plot of SnO electrode cycled in the range of 0.0–1.5 V at the rate of 100 mA/g.

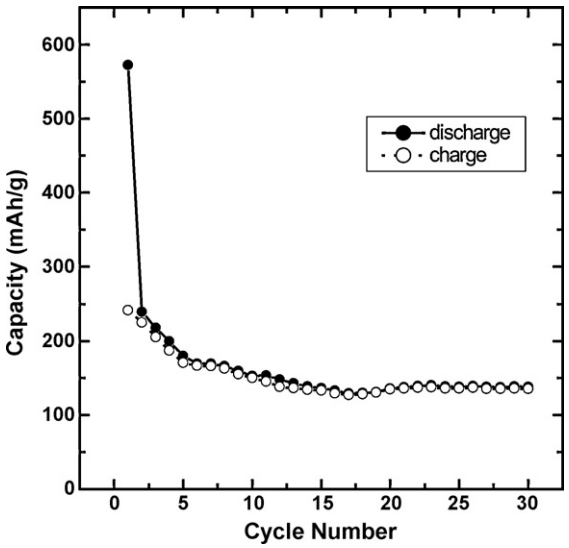

Fig. 9. The capacity vs. cycle number plot of SnO electrode cycled in the range of 0.5–1.5 V at the rate of 100 mA/g.

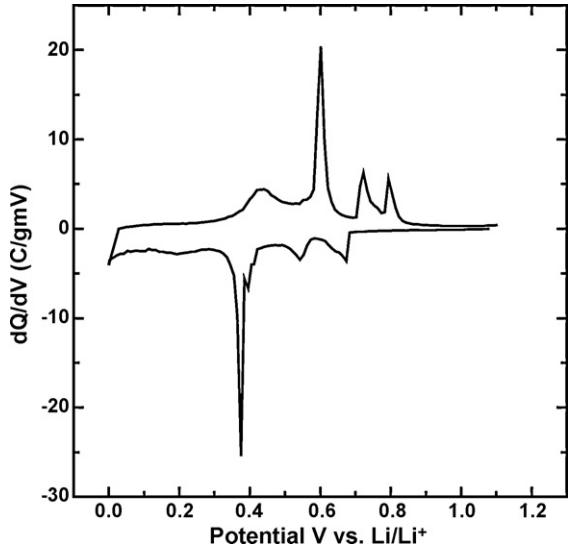

Fig. 10. Derivative capacity plot of SnO electrode after 30 cycling in the range of 0.5–1.5 V at the rate of 100 mA/g.

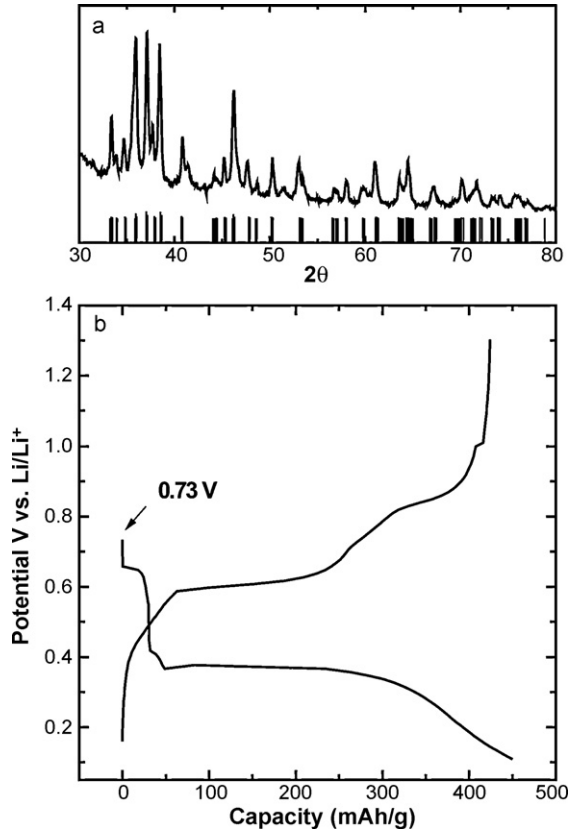

Fig. 11. (a) XRD patterns of LiSn powder and (b) charge/discharge curve of LiSn electrode at the first cycle.

Since the irreversible capacity in Sn and SnO electrode is attributed to the incomplete removal of Li from Sn during charging, it is worthwhile to investigate electrochemical behavior of Li–Sn alloy electrode which contains Li initially. Fig. 11 shows the XRD pattern from LiSn electrode and its charge–discharge curves. The open circuit voltage is about 0.73 V which is close to the transition potential to the LiSn phase during the first discharge of SnO electrode, although it is not directly shown in Fig. 3. The efficiency of LiSn electrode is ~94% in Fig. 11, but it would be 100% if the effects from conducting/biding agent, e.g., the formation of SEI, are excluded. This result supports that the capacity loss during the first cycle in Sn electrode is due to the residual Li in Sn after charging.

4. Conclusions

Electrochemical behaviors of Sn and SnO anodes are studied and compared. Derivative capacity plots show that the similar Li–Sn alloying/de-alloying reactions occur in SnO and Sn electrodes. $Li_{22}Sn_5$ phase is not observed in the discharge product contrary to the previous reports. There is incomplete removal of Li from Sn after the first charge which causes the capacity loss in Sn electrode at the first cycle. In SnO electrode, the aggregation of Sn makes the electrochemical behavior of SnO electrode similar to that of Sn electrode upon cycling. SnO electrode shows the capacity loss even with 0.5 V lower cutoff voltage due to the residual Li in metallic Sn. The pre-existing Li in LiSn alloy electrode however results in almost 100% cycling efficiency at the first cycle.

Acknowledgement

This work was supported by the Energy Efficiency & Resources of the Korea Institute of Energy Technology Evaluation and Planning (KETEP) grant funded by the Korea government Ministry of Knowledge Economy (Project No. = 2008EEL11P070000).

References

[1] I. Rom, M. Wachtler, I. Papst, M. Schmied, J.O. Besenhard, F. Hofer, M. Winter, Solid State Ionics 143 (1999) 329–336.
[2] M. Winter, J.O. Besenhard, Electrochim. Acta 45 (1999) 31–50.
[3] I.A. Courtney, J.R. Dahn, J. Electrochem. Soc. 144 (1997) 2045–2052.
[4] Y. Idota, T. Kubota, A. Matsufuji, Y. Maekawa, T. Miyasaka, Science 276 (1997) 1395–1397.
[5] T. Brousse, R. Retoux, U. Herterich, D.M. Schleich, J. Electrochem. Soc. 145 (1998) 1–4.
[6] J. Chouvin, C. Branci, J. Sarradin, J. Olivier-Fourcade, J.C. Jumas, B. Simon, Ph. Biensan, J. Power Sources 81–82 (1999) 277–281.
[7] I.A. Courtney, R.A. Dunlap, J.R. Dahn, Electrochim. Acta 45 (1999) 51–58.
[8] I. Sandu, T. Brousse, D.M. Schleich, M. Danot, J. Solid State Chem. 177 (2004) 4332–4340.
[9] A. Sivashanmugam, T. Prem Kumar, N.G. Renganathan, S. Gopukumar, M. Wohlfahrt-Mehrens, J. Garche, J. Power Sources 144 (2005) 197–203.
[10] H. Uchiyama, E. Hososno, I. Honma, H. Zhou, H. Imai, Electrochem. Commun. 10 (2008) 52–55.
[11] A. Fernandez, F. Martin, J. Morales, J.R. Ramos-Barrado, L. Sanchez, Electrochim. Acta 51 (2006) 3391–3398.
[12] S. Yang, P.Y. Zavalij, M.S. Whittingham, Electrochem. Commun. 5 (2003) 587–590.
[13] M. Inaba, T. Uno, A. Tasaka, J. Power. Sources 146 (2005) 473–477.
[14] J. Chouvin, J. Olivier-Fourcade, J.C. Jumas, B. Simon, Ph. Biensan, F.J. Fernandez Madrigal, J.L. Tirado, C. Perez Vicente, J. Electroanal. Chem. 494 (2000) 136–146.